

MIT Open Access Articles

First-principles design of nanostructured hybrid photovoltaics based on layered transition metal phosphates

The MIT Faculty has made this article openly available. **Please share** how this access benefits you. Your story matters.

Citation: Lentz, Levi C. and Kolpak, Alexie M. "First-Principles Design of Nanostructured Hybrid Photovoltaics Based on Layered Transition Metal Phosphates." Scientific Reports 7, no. 1 (April 2017): 1248 © 2017 The Author(s)

As Published: <http://dx.doi.org/10.1038/s41598-017-01296-0>

Publisher: Nature Publishing Group

Persistent URL: <http://hdl.handle.net/1721.1/110168>

Version: Final published version: final published article, as it appeared in a journal, conference proceedings, or other formally published context


Terms of use: Creative Commons Attribution 4.0 International License



SCIENTIFIC REPORTS

OPEN

First-principles design of nanostructured hybrid photovoltaics based on layered transition metal phosphates

Levi C. Lentz  & Alexie M. Kolpak

The performance of bulk organic and hybrid organic-inorganic heterojunction photovoltaics is often limited by high carrier recombination arising from strongly bound excitons and low carrier mobility. Structuring materials to minimize the length scales required for exciton separation and carrier collection is therefore a promising approach for improving efficiency. In this work, first-principles computations are employed to design and characterize a new class of photovoltaic materials composed of layered transition metal phosphates (TMPs) covalently bound to organic absorber molecules to form nanostructured superlattices. Using a combination of transition metal substitution and organic functionalization, the electronic structure of these materials is systematically tuned to design a new hybrid photovoltaic material predicted to exhibit very low recombination due to the presence of a local electric field and spatially isolated, high mobility, two-dimensional electron and hole conducting channels. Furthermore, this material is predicted to have a large open-circuit voltage of 1.7V. This work suggests that hybrid TMPs constitute an interesting class of materials for further investigation in the search for achieving high efficiency, high power, and low cost photo Zirconium phosphate was chosen, in part, due to previous experiment voltaics.

Photovoltaic (PV) devices based on organic or hybrid organic-inorganic materials are of interest because of their low cost, low environmental impact, and structural flexibility, among a range of other scientific and engineering applications. However, current organic and hybrid PV devices have relatively low efficiencies compared to state-of-the-art silicon PV due to high exciton recombination rates and/or low open-circuit voltage (V_{OC}). In general, the former is due to trap states within the material as well as interfacial recombination centers, while the latter is a result of non-optimal band alignment.

Bulk heterojunctions (BHJs), composed of donor and acceptor molecules, are one approach to addressing these challenges. In BHJs, deposition is focused on maximizing the surface area between the donor and acceptor molecules to increase the probability of charge separation. Further, manufacturing methods allow for thin film deposition, decreasing overall feature lengths. However, the atomic-scale disorder at the donor-acceptor junctions often leads to high densities of interfacial states that act as recombination centers. These mid-gap states may also lead to a decrease in the overall V_{OC} . In this work we present a framework that utilizes layered materials to leverage existing organic molecules in a way that minimizes recombination centers and maximizes both exciton separation and V_{OC} .

Previous efforts to increase V_{OC} in BHJs have generally focused on two approaches: (i) controlling morphology, often by employing carbon nanotube scaffolds^{1,2} or nanostructured surfaces^{3,4} and/or (ii) incorporating multiple acceptor layers to optimize band alignment between donor, acceptor, and electrode⁵. Efficiency gains have also been achieved using ferroelectric materials that may create a net dipole between the electrodes of the device^{6,7}. The improvements due to these approaches, however, may be offset by atomic-scale disorder that leads to high exciton recombination rates at the various interfaces within the device.

To address these issues, we propose a new class of nanostructured hybrid organic-inorganic photovoltaics composed of layered transition metal phosphates (TMPs) covalently bound to organic absorber molecules to

Department of Mechanical Engineering, Massachusetts Institute of Technology, 77 Massachusetts Ave, Cambridge, MA, 02139, USA. Correspondence and requests for materials should be addressed to A.M.K. (email: kolpak@mit.edu)

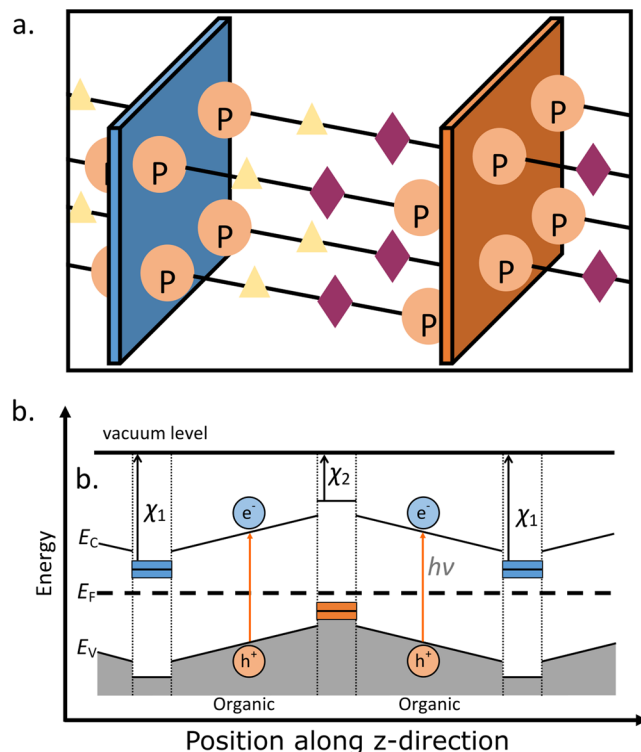


Figure 1. (a) Schematic of the proposed atomic structure, in which alternating inorganic hole and electron transport layers (blue and orange sheets, respectively) are separated by polar organic absorber molecules. Triangles and diamonds represent organic functional groups chosen to tune the polarization and the band alignment. (b) Schematic band energy diagram corresponding to the structure in (a). χ_1 and χ_2 are the electron affinities of the inorganic electron and hole conducting layers, respectively.

form nanostructured superlattices. Crystalline, layered TMP superlattices of this type have been previously synthesized using solution-based processing methods⁸, but to date have not been widely investigated in the context of electronic or optical applications. Our recent work suggests high tunability of TMP band energies through simple surface functionalization⁹. Using these relationships, we optimize a new hybrid TMP-organic superlattice based on zirconium phosphate, α -Zr(HPO₄)₂, one of the most well-studied layered TMPs, and we show that this new material is predicted to exhibit very low exciton recombination, high electron and hole mobilities, and a large open-circuit voltage of 1.7 eV.

Approach

Nanostructured PV Design. The proposed material architecture is illustrated schematically in Fig. 1. In this architecture, planar organic molecules link 2D inorganic sheets with nanoscale separation. The 2D inorganic sheets have large band gaps, so excitons are generated only within the organic regions. As shown in the schematic band diagram in Fig. 1b, these excitons are separated via an electric field, which is determined by a combination of the dipole of the polar organic molecule and the electron affinity differences between the inorganic layers. The characteristic length scale over which this dipole acts (the distance between adjacent inorganic sheets) is on the order of 1–10 nanometers. Small length scale polarity such as this has been demonstrated in the surface functionalization of 2D sheets to dissociate water molecules¹⁰. This length scale enables large local electric fields as well as transit length scales that are significantly shorter than the mean free paths of the excitons or the separated charge carriers in typical organic materials. Coupled with appropriate design of the energy band alignment, this ensures that carriers are transferred into the relevant inorganic transport layers, from which there is a significant energy barrier to escape, as illustrated in Fig. 1b. Thus, electrons and holes in the inorganic transport channels have a negligible probability for recombination.

This hypothetical framework may, in principle, be achieved with many different materials combinations. We choose to implement this design using layered TMPs, which have been demonstrated to self-assemble into ordered crystal structures with covalently bound organic materials. As discussed below, the range of both layered TMP compounds and polar organic absorber molecules provides potential for a wide range of materials properties.

Materials Platform. Similar to graphite and transition metal chalcogenides such as MoS₂, bulk layered TMPs are composed of stacks of two-dimensional (2D) crystalline sheets bound primarily via van der Waals interactions along the stacking direction. Solution-based syntheses of TMPs have been demonstrated for a range of chemical compositions⁸ to form ordered, crystalline superlattices composed of alternating inorganic and

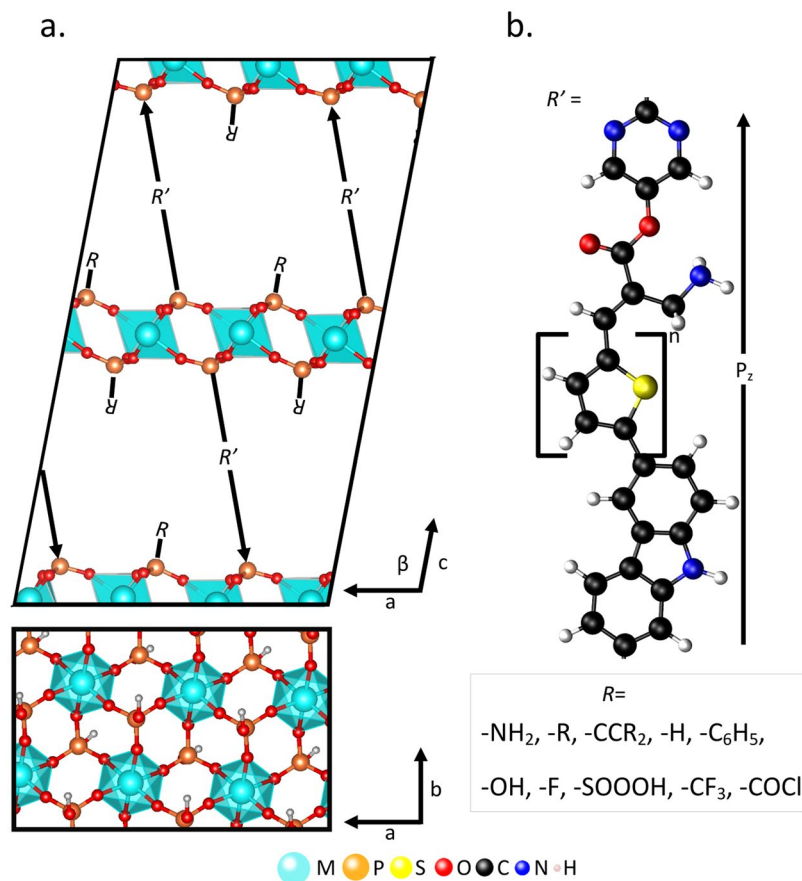


Figure 2. Schematic illustrating the range of structures studied in this work. (a) Top, side view of supercell with R' molecules. Arrows show the direction of molecular dipoles. Bottom, in-plane view of TMP with R = -OH. (b) Representative molecule of R' studied in this work.

organic layers with nanoscale spacing^{11–14}. Experimental measurements of zirconium phosphate show that bulk conductivity can be tuned from about 0.001 to 1 S/cm¹⁵ via intercalation of cations such as Li, Na, and K between the 2D sheets. This conductivity is comparable to or greater than that of many organic materials used in BHJs, such as PEDOT:PSS¹⁶, ITO:PET¹⁷, and P3HT:PCBM¹⁷.

In this work we focus on materials based on α -Zr(HPO₄)₂¹⁸, as illustrated in Fig. 2, with the general composition Zr_{2-x}M_x(RRPO₃)₄, where M is a transition metal substitution at the Zr lattice position, R' is a polar derivative of MK2 (2-cyano-3-[5-(9-ethyl-9H-carbazol-3-yl)-3,3,3,4-tetra-n-hexyl[2,2,5,2,5,2]-quater thiophen-5yl]), an organic molecule that has been used as an absorber in dye-sensitized solar cells¹⁹, and R is a functional group on the TMP. Zirconium phosphate was chosen, in part, due to previous experimental work that has demonstrated ordering of polar dyes using zirconium phosphate as a template²⁰ in a manner similar to that proposed here. As described below, M and R are chosen to optimize the band alignment between the inorganic and organic layers. Atomic structure information for all systems in this work can be found in the Supplementary Information.

The MK2 molecule is modified to increase the polarity of the experimental structure. The large polarity of pyrimidine is exploited in this structure to create a highly polar MK2 molecule, as shown in the top of Fig. 2b. The band edges of MK2 are primarily composed of states from the four thiophene monomers in the central part of the molecule. The experimental HOMO-LUMO gap of this molecule is approximately 2 eV, although this can be modified by varying the length of the polythiophene chain²¹.

The polarity of the organic molecule is given by $P = \frac{D}{V}$, where D is the dipole of the molecule and V is the volume occupied by the molecule in the supercell. This polarization leads to an electric field, $E_{field} = \frac{P}{2\epsilon_r\epsilon_0}$, where ϵ_r is the relative permittivity of the organic molecule, ϵ_0 is the permittivity of free space, and the factor of 1/2 is due to the void fraction of the MK2 molecule in the superlattice. This constant field imposes a rigid energetic shift between alternating inorganic layers. In order to separate excitons, we require this field to be greater than E_b , the exciton binding energy in the organic material. While E_b has not been directly calculated or measured in this work, using well studied trends in organic molecules²², the binding energy in MK2 is estimated to be on the order of 0.5–1 eV.

To optimize the energy alignment of the organic and inorganic layers so that there are no barriers for electron (hole) transfer from the organic region into the inorganic electron (hole) conducting layer, we use relationships identified in our previous work to independently tune the band gap and the energies of the band edges in the

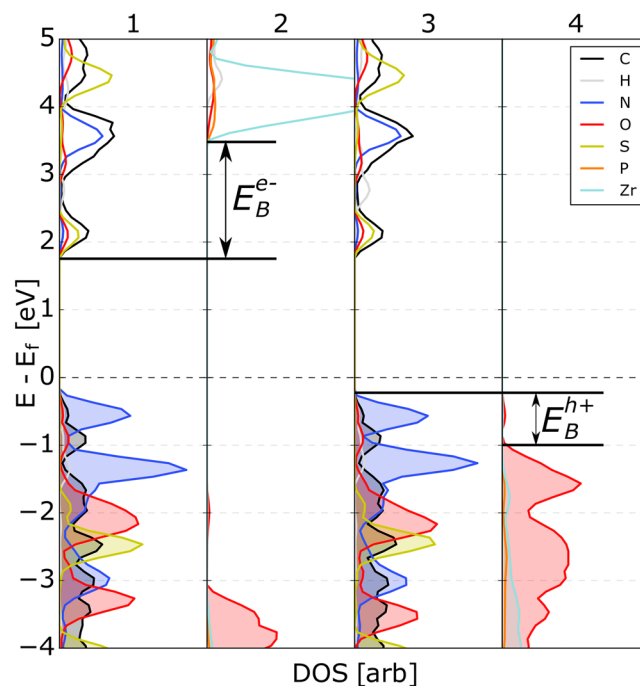


Figure 3. Atom-projected DOS of the TMP-organic superlattice with $R = -\text{OH}$ and $M = \text{Zr}$. The DOS of the organic regions are shown in panels 1 and 3, while panels 2 and 4 show the TMP layers. In this case, the composition of adjacent inorganic layers are the same; the shift in the DOS from panel 2 to 4 is due solely to the polarity of the organic molecules.

alternating TMP layers⁹. In particular, large variations in the band gap can be obtained via in-plane cation substitution, while independent and precise control of the energies of the band edges is achieved through substitution of the out-of-plane $-R$ functional groups. Through selection of cation substitution and $-R$ functional group, the energetic barriers between the organic layer and the inorganic sheets can be minimized, maximizing V_{OC} .

Discussion

In Fig. 3, the projected density of states (pDOS) of the reference system with $R = -\text{OH}$ and $M = \text{Zr}$ is shown; in this case, the composition of all of the inorganic layers is the same. Creating a superlattice with organic molecules connecting this TMP sheet energetically shifts the CBM/VBM by 2.16 eV, as indicated by shift in the pDOS in panels 2 and 4 of Fig. 3. This gives an electric field across the MK2 molecule of $42.8 \text{ mV}\text{\AA}^{-1}$. The isolated MK2 molecule was found to have a dipole of 7.95 D, creating a polarization of $1.032 \mu\text{Ccm}^{-2}$, and the relative permittivity of thiophene is 2.8, giving an electric field $E = P/2\epsilon\epsilon_0 = 38 \text{ mV}\text{\AA}^{-1}$, in good agreement with that calculated from DFT. The small difference is likely a result of using the permittivity of thiophene as an approximation for that of the MK2 molecule. The exciton binding energy in polythiophene is 0.18 eV^{23} , and typical binding energies in organic molecules are in the range $0.1\text{--}1 \text{ eV}^{22}$, thus, the computed field will be sufficient to separate excitons in these materials.

As Fig. 3 shows, there is a large barrier of about 1.86 eV (E_B^{e-} in panel 2) for electron transfer from the conduction band edge of the organic regions (panels 1 and 3) into the conduction band edge of the inorganic electron transport layer in the reference system. There is also a barrier of 0.81 eV (E_B^{h+} in panel 4) for hole transfer from the valence band edge of the organic to the that of the hole conducting layer. Despite the electric field, these barriers will trap the free carriers within the organic region. Extracting the charge carriers while concurrently maximizing V_{OC} requires that both E_B^{e-} and E_B^{h+} are close to zero.

To further tune the band alignment to achieve this requirement, we substitute the $-\text{OH}$ groups on the surface of each of the $\text{Zr}(\text{HPO}_4)_4$ layers with different functional groups. Building off of previously demonstrated surface functionalization substitution⁹, we replace these $-\text{OH}$ groups with a range of organic groups. Figure 4 shows the effects of $-R$ substitution on the valence and conduction band edges of $\text{Zr}(\text{RPO}_3)_2$. As the figure shows, the energies of both the valence and conduction band edges vary linearly with respect to the Hammett constant²⁴ (a measure of the electron withdrawing or donating character of a substituent often used in organic chemistry) of the functional group, while the magnitude of the band gap remains approximately constant for all $-R$.

To achieve the desired alignment of the valence band edge (VBE) of the organic absorber and TMP hole conducting layer, we require an upward shift of approximately 0.8 eV in the VBE of the latter. Referring to Fig. 4, this can be achieved by substituting the $-\text{OH}$ functional group with $-\text{NH}_2$. However, the barrier for electron transfer between the organic and TMP electron conducting layers is larger than the range of energies shown in Fig. 4. As we showed in previous work, we can systematically tune the band gap of the TMP layer by substituting some of the Zr with other transition metals⁹. Combining the observed trends for cation substitution and surface

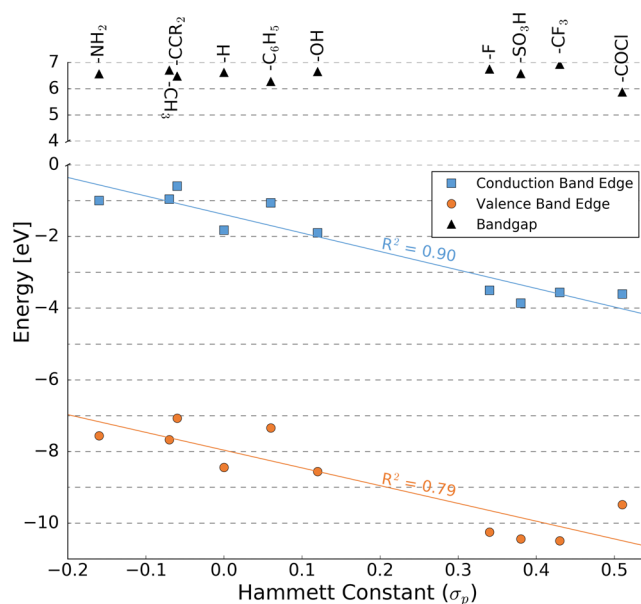


Figure 4. Linear relationships between band gap, electron affinity, and ionization potential and the Hammett constant of the functional group R .

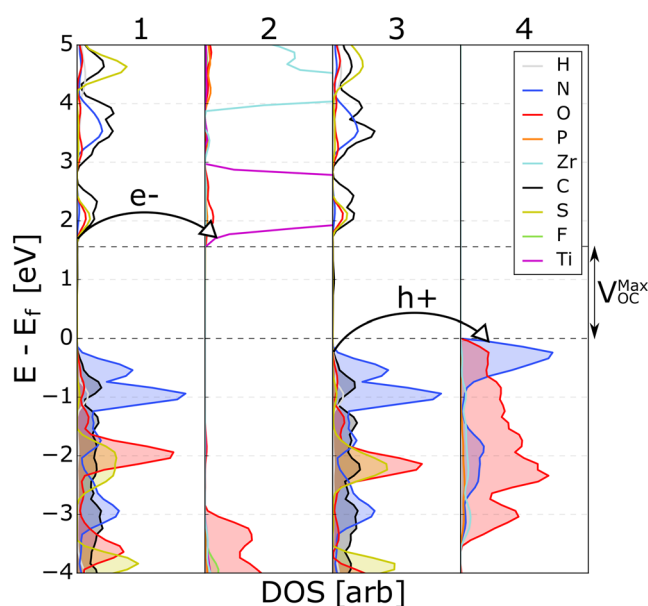


Figure 5. The pDOS of the different layers in the modified organic region. Panels 1 and 3 are the unmodified organic regions, panel 2 is $ZrTi(PO_3)_2$, and panel 4 is $Zr(NH_2PO_3)_2$. In this configuration, there is no hole barrier between panels 1,2 and 3,4 allowing charge extraction from the organic regions. The predicted $V_{OC,max}$ of this system is 1.7 eV.

modification, we find that substitution of half of the Zr with Ti in addition to substitution of -OH with -F will shift the conduction band edge (CBE) of the electron conducting layer into good alignment with the CBE of the organic layer. We note that, due to the origins of the engineered band shifts, large amounts of exchange of the different R groups between the TMP layers will alter the predicted band alignment; however, low concentrations of R group disorder should not have a significantly affect the overall band alignment.

The overall bulk material, shown in Fig. 6, can be written as $Zr_{0.5}Ti_{0.5}(R_{0.5}F_{0.5}PO_3)_2-Zr(R_{0.5}(NH_2)_{0.5}PO_3)_2$, where $-R$ is the modified polar MK2 molecule. The pDOS of this system is shown in Fig. 5. The computed energy levels are in good agreement with the alignment predicted using the trends in band gap and VBE/CBE discussed above. We find that this system has a V_{OC} of 1.71 eV, a relatively small decrease with respect to the maximum possible value of 2 eV, the band gap of organic absorber. Excitons generated in the organic absorber (panels 1 and 3 in Fig. 5) are effectively separated due to the large electric field, and holes and electrons are driven to the relevant TMP layers (panels 2 and 4, respectively, in Fig. 5).

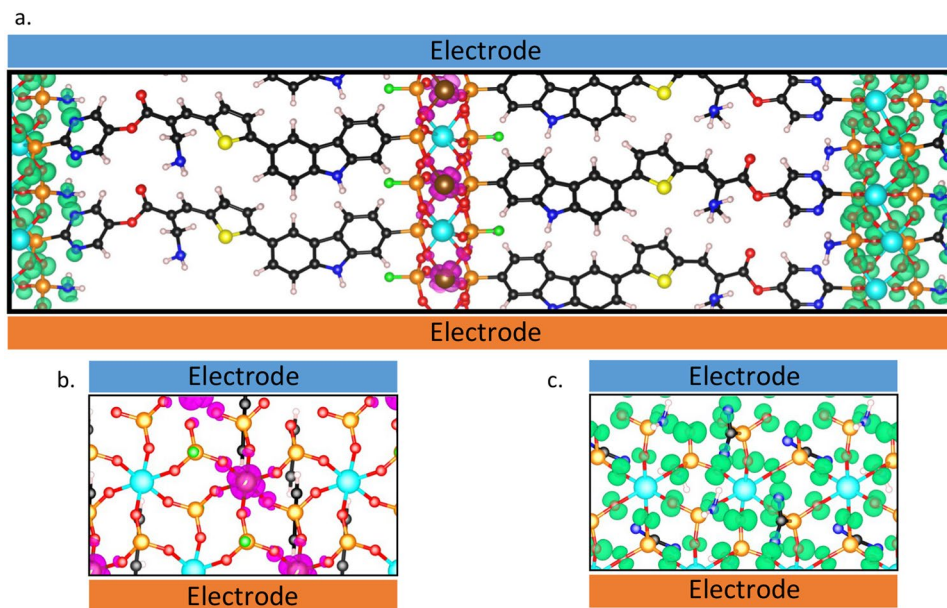


Figure 6. (a) The xz -plane of the bulk system showing spatial localization of the density of states at the conduction band edge (purple) and the valence band edge (green), states are highly localized outside the organic region, implying that the exciton is spatially separated in this system. (b) The xy -plane of the electron extracting layer and (c). The xy -plane of the hole extracting layer.

Figure 6, shows the states corresponding to the CBM and VBM of the system. As the figure illustrates, these states are spatially localized in alternating inorganic sheets, with little amplitude in the organic region. This further decreases the probability for electron-hole recombination. Using the computed density of states and the Boltzmann transport equation, we estimate the in-plane effective masses in the electron and hole conducting inorganic layers. We find that the in-plane effective mass in the electron conducting inorganic layer is 3.7, while the in-plane hole mass in the hole conducting layer is 4.2. Effective masses have been normalized by the mass of a free electron. Out-of-plane effective masses are 109.8 and 43.6 for the electron and hole layers, respectively, indicating free charge carriers will not be able to travel normal to their respective sheet, further preventing recombination. These values suggest these layers are sufficiently conducting to facilitate charge carrier extraction to the electrodes.

Conclusions

In conclusion, we have presented a new approach for the design of hybrid organic-inorganic photovoltaics with low carrier recombination and large open-circuit voltage. We have demonstrated that layered transition metal phosphates provide a highly tunable framework for realizing such materials, and we have predicted a specific new material, based on zirconium phosphate covalently bound to a derivative of a known dye-sensitizing molecule, MK2, that forms an ordered organic-inorganic bulk superlattice with nanostructured dimensions.

We predict that this material has a large open-circuit voltage of 1.7 eV and, further, will exhibit low carrier recombination due to a combination of large local electric fields, nanoscale carrier diffusion distances, spatially localized conduction and valence band edge states, and relatively high mobility electron and hole conducting layers. This work suggests that hybrid TMPs are an exciting class of materials for further investigation in the search for achieving high efficiency, high power, and low cost photovoltaics.

Computational Details. All structure optimization and electronic structure calculations were performed using the plane-wave DFT package Quantum Espresso (QE)²⁵ using the GGA-PBE formulation of the exchange-correlation^{26,27}, ultrasoft pseudopotentials²⁸, and the Grimme van der Waals correction^{29,30}. All pseudopotentials were obtained from existing QE libraries and tested by comparing computed and experimental structural properties of the relevant ground state elemental phases and bulk TMPs at standard temperature and pressure. All calculations were performed with an energy cutoff of 800 eV, and forces on all atoms were converged to less than 10 meV/Å. Ionization potentials and electron affinities were determined by referring the band energies of the 2D sheets to the energy of the vacuum using a 25 Å separation between periodic copies in the direction perpendicular to the plane of the 2D sheet. The GGA+ U formalism³¹ was used in the hybrid TMP-organic systems. The value of U was chosen such that the band gap in the TMP region agreed with that computed for the bulk TMP using high accuracy GW calculations⁹. The polarity of isolated molecules was computed using the Quantum Chemistry package NWChem³². As GW calculations of the full hybrid organic-TMP system are computationally intractable, all band alignments were determined under the approximation of fixing the band gap of the organic region to the experimental value of 2 eV by shifting the CMB of the organic layer to replicate the experimental gap. Band edges in the inorganic layers were corrected in a similar fashion: CBM energies were rigidly shifted to replicate the GW band gap. This approach was chosen as DFT is known to underestimate the energy levels of

excited states in the system, while representing the occupied states accurately. No other changes were made to the nature of the DOS of the studied systems.

Conductivities were determined using the Boltzmann transport equations using the BoltzTraP³³ code to compute the conductivity tensor in terms of the scattering time. As conductivities of TMPs are not well studied, the scattering time is not known. As such, this was used with the density of states to calculate the curvature of the band edges in terms of a free electron mass. This was verified through direct computation of the curvature of the band edges and using the effective mass approximation. Reported in-plane effective masses are the average of the along the in-plane principle directions (here as the crystallographic *a* and *b* directions). Out-of-plane curvatures are calculated normal to the plane of the TMP.

References

- Li, C. *et al.* A fullerene-single wall carbon nanotube complex for polymer bulk heterojunction photovoltaic cells. *J. Mater. Chem.* **17**, 2406–2411, doi:10.1039/B618518E (2007).
- Kymakis, E., Alexandrou, I. & Amarutunga, Ga. J. High open-circuit voltage photovoltaic devices from carbon-nanotube-polymer composites. *J. Appl. Phys.* **93**, 1764–1768, doi:10.1063/1.1535231 (2003).
- Park, S. H. *et al.* Bulk heterojunction solar cells with internal quantum efficiency approaching 100%. *Nat. Photonics* **3**, 297–302, doi:10.1038/nphoton.2009.69 (2009).
- Brabec, C. J. *et al.* Origin of the open circuit voltage of plastic solar cells. *Adv. Funct. Mater.* **11**, 374–380, doi:10.1002/(ISSN)1616-3028 (2001).
- Chuang, C.-H. M., Brown, P. R., Bulović, V. & Bawendi, M. G. Improved performance and stability in quantum dot solar cells through band alignment engineering. *Nat. Mater.* **13**, 796–801, doi:10.1038/nmat3984 (2014).
- Nalwa, K. S. *et al.* Enhanced charge separation in organic photovoltaic films doped with ferroelectric dipoles. *Energy Environ. Sci.* **5**, 7042–7049, doi:10.1039/c2ee03478f (2012).
- Yuan, Y. *et al.* Efficiency enhancement in organic solar cells with ferroelectric polymers. *Nat. Mater.* **10**, 296–302, doi:10.1038/nmat2951 (2011).
- Clearfield, A. & Konstantinos, D. Metal Phosphonate Chemistry (Royal Society of Chemistry, 2011).
- Lentz, L. C., Kolb, B. & Kolpak, A. M. Control of valence and conduction band energies in layered transition metal phosphates via surface functionalization. *Phys. Chem. Chem. Phys.* **18**, 14122–14128, doi:10.1039/c6cp00994h (2016).
- Li, X., Li, Z. & Yang, J. Proposed Photosynthesis Method for Producing Hydrogen from Dissociated Water Molecules Using Incident Near-Infrared Light. *Phys. Rev. Lett.* **112**, 018301, doi:10.1103/PhysRevLett.112.018301 (2014).
- Vivani, R., Alberti, G., Costantino, F. & Nocchetti, M. New advances in zirconium phosphate and phosphonate chemistry: Structural archetypes. *Microporous Mesoporous Mater.* **107**, 58–70, doi:10.1016/j.micromeso.2007.02.029 (2008).
- Lei, X., Wang, L., Cui, Z., Xu, S. & Zhang, F. Preparation of zirconium phenylphosphonate films with different crystallite orientations on polystyrene substrates by *in situ* hydrothermal crystallization. *Thin Solid Films* **519**, 3552–3556, doi:10.1016/j.tsf.2011.01.246 (2011).
- Clearfield, A. & Wang, Z. Organically pillared microporous zirconium phosphonates. *J. Chem. Soc. Dalton Trans.* 2937–2947, doi:10.1039/B202371G (2002).
- Wong, M. *et al.* Large-scale self-assembled zirconium phosphate smectic layers via a simple spray-coating process. *Nat. Commun.* **5** (2014).
- Sadaoka, Y., Matsuguchi, M., Sakai, Y. & Mitsui, S. Electrical properties of α -zirconium phosphate and its alkali salts in a humid atmosphere. *J. Mater. Sci.* **23**, 2666–2675, doi:10.1007/BF00547435 (1988).
- Xia, Y. & Ouyang, J. Significant Conductivity Enhancement of Conductive Poly(3,4-ethylenedioxythiophene): Poly(styrenesulfonate) Films through a Treatment with Organic Carboxylic Acids and Inorganic Acids. *ACS Appl. Mater. Interfaces* **2**, 474–483 (2010).
- Na, S.-I., Kim, S.-S., Jo, J. & Kim, D.-Y. Efficient and Flexible ITO-Free Organic Solar Cells Using Highly Conductive Polymer Anodes. *Adv. Mater.* **20**, 4061–4067, doi:10.1002/adma.v20:21 (2008).
- Alberti, G., Costantino, U., Millini, R., Perego, G. & Vivani, R. Preparation, Characterization, and Structure of α -Zirconium Hydrogen Phosphate Hemihydrate. *J. Solid State Chem.* **113**, 289–295, doi:10.1006/jssc.1994.1373 (1994).
- Hara, K., Wang, Z.-S., Cui, Y., Furube, A. & Koumura, N. Long-term stability of organic-dye-sensitized solar cells based on an alkyl-functionalized carbazole dye. *Energy Environ. Sci.* **2**, 1109–1114, doi:10.1039/b907486d (2009).
- Katz, H. E. *et al.* Polar Orientation of Dyes in Robust Multilayers by Zirconium Phosphate-Phosphonate Interlayers. *Science* **254**, 1485–1487, doi:10.1126/science.254.5037.1485 (1991).
- Chain-length dependence of electronic and electrochemical properties of conjugated systems: polyacetylene, polyphenylene, polythiophene, and polypyrrole - Journal of the American Chemical Society (ACS Publications). Available at: <http://pubs.acs.org/doi/abs/10.1021/ja00360a004> (Accessed: 13th October 2015).
- Knupfer, M. Exciton binding energies in organic semiconductors. *Appl. Phys. A* **77**, 623–626, doi:10.1007/s00339-003-2182-9 (2003).
- Köse, M. E. Evaluation of Acceptor Strength in Thiophene Coupled Donor–Acceptor Chromophores for Optimal Design of Organic Photovoltaic Materials. *J. Phys. Chem. A* **116**, 12503–12509, doi:10.1021/jp309950f (2012).
- Hansch, C., Leo, A. & Taft, R. W. A survey of Hammett substituent constants and resonance and field parameters. *Chem. Rev.* **91**, 165–195, doi:10.1021/cr00002a004 (1991).
- Giannozzi, P. *et al.* QUANTUM ESPRESSO: a modular and open-source software project for quantum simulations of materials. *J. Phys. Condens. Matter* **21**, 395502, doi:10.1088/0953-8984/21/39/395502 (2009).
- Perdew, J. P., Burke, K. & Ernzerhof, M. Generalized Gradient Approximation Made Simple. *Phys. Rev. Lett.* **77**, 3865–3868, doi:10.1103/PhysRevLett.77.3865 (1996).
- Perdew, J. P. *et al.* Atoms, molecules, solids, and surfaces: Applications of the generalized gradient approximation for exchange and correlation. *Phys. Rev. B* **46**, 6671–6687, doi:10.1103/PhysRevB.46.6671 (1992).
- Vanderbilt, D. Soft self-consistent pseudopotentials in a generalized eigenvalue formalism. *Phys. Rev. B* **41**, 7892–7895, doi:10.1103/PhysRevB.41.7892 (1990).
- Grimme, S. Semiempirical GGA-type density functional constructed with a long-range dispersion correction. *J. Comput. Chem.* **27**, 1787–1799, doi:10.1002/jcc.20495 (2006).
- Barone, V. *et al.* Role and effective treatment of dispersive forces in materials: Polyethylene and graphite crystals as test cases. *J. Comput. Chem.* **30**, 934–939, doi:10.1002/jcc.v30:6 (2009).
- Anisimov, V. I., Zaanen, J. & Andersen, O. K. Band theory and Mott insulators: Hubbard U instead of Stoner I. *Phys. Rev. B* **44**, 943–954, doi:10.1103/PhysRevB.44.943 (1991).
- Valiev, M. *et al.* NWChem: A comprehensive and scalable open-source solution for large scale molecular simulations. *Comput. Phys. Commun.* **181**, 1477–1489, doi:10.1016/j.cpc.2010.04.018 (2010).
- Madsen, G. K. H. & Singh, D. J. BoltzTraP. A code for calculating band-structure dependent quantities. *Comput. Phys. Commun.* **175**, 67–71, doi:10.1016/j.cpc.2006.03.007 (2006).

Acknowledgements

Research supported as part of S³TEC, an Energy Frontier Research Center (EFRC) funded by the U.S. Department of Energy (DOE), Office of Science, Basic Energy Sciences (BES), under Award DE-SC0001299/DE-FG02-09ER46577.

Author Contributions

L.C.L. performed all calculations. L.C.L. and A.M.K. analyzed the data and prepared the manuscript.

Additional Information

Supplementary information accompanies this paper at doi:[10.1038/s41598-017-01296-0](https://doi.org/10.1038/s41598-017-01296-0)

Competing Interests: The authors declare that they have no competing interests.

Publisher's note: Springer Nature remains neutral with regard to jurisdictional claims in published maps and institutional affiliations.



Open Access This article is licensed under a Creative Commons Attribution 4.0 International License, which permits use, sharing, adaptation, distribution and reproduction in any medium or format, as long as you give appropriate credit to the original author(s) and the source, provide a link to the Creative Commons license, and indicate if changes were made. The images or other third party material in this article are included in the article's Creative Commons license, unless indicated otherwise in a credit line to the material. If material is not included in the article's Creative Commons license and your intended use is not permitted by statutory regulation or exceeds the permitted use, you will need to obtain permission directly from the copyright holder. To view a copy of this license, visit <http://creativecommons.org/licenses/by/4.0/>.

© The Author(s) 2017